Journal of Applied Polymer Science

Synthesis, antimicrobial, and release behaviors of tetracycline hydrochloride loaded poly (vinyl alcohol)/chitosan/ZrO_2 nanofibers

Hualin Wang,[1,2] Chengjiang Chu,[1] Lilan Hao,[1] Yi She,[1] Yanan Li,[1] Linfeng Zhai,[1] Shaotong Jiang[2,3]
[1]School of Chemistry and Chemical Technology, Hefei University of Technology, Hefei, Anhui 230009, People's Republic of China
[2]Anhui Institute of Agro-Products Intensive Processing Technology, Hefei, Anhui 230009, People's Republic of China
[3]School of Biotechnology and Food Engineering, Hefei University of Technology, Hefei, Anhui 230009, People's Republic of China
Correspondence to: H. Wang (E-mail: hlwang@hfut.edu.cn)

ABSTRACT: Tetracycline hydrochloride loaded poly (vinyl alcohol)/chitosan/ZrO_2 (Tet-PVA/CS/ZrO_2) hybrid nanofibers were fabricated *via* electrospinning technique. The representative weight ratio of PVA/CS at 3 : 1 was chosen to fabricate drug carrier PVA/CS/ZrO_2 nanofibers. The drug carrier showed a decrease in average diameter with the increase of ZrO_2 content at given conditions, and the nanofibers were uneven and interspersed with spindle-shape beads with ZrO_2 content at 60 wt % and above. The networks linked by hydrogen and Zr–O–C bonds among PVA, CS, and ZrO_2 units resulted in the improving of thermal stability and decreasing of crystallinity of the polymeric matrix. Moreover, the incorporation of ZrO_2 endowed the fibers with ultraviolet shielding effect ranged from 200 to 400 nm. The Tet loading dosage had no obvious effect on the morphology and size of the medicated nanofibers at Tet content below 8 wt %, but interspersed with spindle-shaped beads when Tet content increased to 10 wt %. The Tet-PVA/CS/ZrO_2) nanofibers showed well controlled release and better antimicrobial activity against *Staphylococcus aureus*, and the Tet release from the medicated nanofibers could be described by Fickian diffusion model for $M_t/M_\infty < 0.6$. These medicated nanofibers may have potential as a suitable material in drug delivery and wound dressing. © 2015 Wiley Periodicals, Inc. J. Appl. Polym. Sci. **2015**, *132*, 42506.

KEYWORDS: composites; drug delivery systems; electrospinning

Received 18 November 2014; accepted 17 May 2015
DOI: 10.1002/app.42506

INTRODUCTION

Electrospinning is a convenient technique to fabricate functional nanofibers and has attracted great interest in recent years.[1–4] Electrospun nanofibers can range from 50 to 500 nm in diameter and show the unique physical and chemical properties.[5,6] For example, nanofibers have a large specific surface area, high surface energy, high activity and can be easily functionalized, which have been widely used in catalyst,[7] sensor,[8] and microelectronics,[9] especially in biomedical materials such as wound dressing,[10,11] drug delivery,[12,13] and tissue engineering.[14,15]

Chitosan (CS), a linear polysaccharide of (1,4)-linked 2-amino-deoxy-β-d-glucan derived from chitin,[16] is available from waste products in shellfish industry,[17] which is a nontoxic biopolymer well known for its biodegradability, biocompatibility,[18] antibacterial ability, and blood clotting.[19] However, the application of pure CS has been limited because of the problems associated with its performance such as brittleness and moisture barrier nature.[20] It is well known that poly (vinyl alcohol) (PVA) has been often used as a basic material for different applications in biomedical field because of its nontoxicity, biocompatibility and biodegradability.[21,22] In addition, PVA has significant spinnability and film-forming ability. Nevertheless, the deficiencies of weak resistant to acids and poor thermal stability limit the application of PVA fibers to some extent. As biomedical material, CS/PVA blend nanofibers or nanofibrous membranes have attracted special attention.[5,23,24] It is an effective way to improve system properties or endow novel functions for polymer by incorporating inorganic nanoparticles into the polymer matrix.[25,26] As expected, the incorporation of ZrO_2 sol can improve the thermal stability of polymer.[27] Especially, ZrO_2 nanoparticles can stimulate nerve tissue and enhance human immunity as a kind of far-infrared materials.[28]

In the present work, tetracycline hydrochloride (Tet) was used as a model drug and a representative gram-positive bacterium *Staphylococcus aureus* (*S. aureus*) was chosen as test bacterium. Tet loaded PVA/CS/ZrO_2 (Tet-PVA/CS/ZrO_2) hybrid nanofibers were fabricated *via* electrospinning technique. The influence of the weight ratio of PVA/CS on the viscosity, conductivity, and fiber formability of the blend solution was investigated. The effects of ZrO_2 and the Tet content on the morphology of the nanofibers, the structure, thermal stability, ultraviolet

absorbability, and *in vitro* degradation for drug carrier PVA/CS/ZrO_2 hybrid nanofibers were explored. The release behavior and antimicrobial activity of Tet-PVA/CS/ZrO_2 nanofibers were evaluated.

EXPERIMENTAL

Materials

PVA with the degree of polymerization at 1700 and hydrogen peroxide (H_2O_2, 30%) were purchased from Sinopharm Chemical Reagent (Shanghai, China). Zirconyl chloride octahydrate ($ZrOCl_2{\cdot}8H_2O$) was purchased from Aldrich Chemical (Milwaukee, WI). CS (Mw 300 kDa, DD 95%) was purchased Zhejiang Aoxing Biochemical (Zhejiang, China). Tet was obtained from Sigma (St. Louis, MO). *S. aureus* was harvested from School of Biological and Food Engineering, Hefei University of Technology (Anhui, China). All the other chemical solvents were purchased from Sinopharm Chemical Reagent (Shanghai, China).

Preparation of Samples

Zirconia (ZrO_2) sol was prepared from $ZrOCl_2{\cdot}8H_2O$ by sol-gel method.[27] PVA solution (10 wt %) was obtained by dissolving PVA in distilled water at 95°C. Meanwhile, CS was dissolved into 2.0% (v/v) acetic acid to prepare 8 wt % CS solution assisted with magnetic stirring. Subsequently, a series of PVA/CS electrospun solutions (weight ratios of PVA/CS were employed at 1 : 1, 2 : 1, 3 : 1, and 4 : 1) were prepared by blending PVA solution with CS solution at room temperature under constant stirring for 1 h. The required ZrO_2 sol was added into PVA/CS blend solution to obtain PVA/CS/ZrO_2 electrospun solution (ZrO_2 contents were employed at 0, 20, 40, and 60 wt %, all based on the weight of PVA).

On the basis of experimental data, the representative PVA/CS/ZrO_2 solution with PVA/CS weight ratio at 3 : 1 and ZrO_2 content at 40 wt % was chosen to prepare Tet-PVA/CS/ZrO_2 nanofibers. The electrospun solution was obtained by adding Tet into PVA/CS/ZrO_2 solution (Tet contents were employed at 0, 2, 4, 6, 8, and 10 wt %, all based on the weight of PVA).

Electrospinning Procedures

The electrospinning device was consisted of a syringe, a needle (0.41 mm internal diameter), a copper sheet, a ground electrode, and a high-voltage power supply (DW-P403-1ACCC, Tianjin Dongwen, China). On the basis of experimental data, electrospinning processing was carried out at room temperature with a relative humidity (RH) at 50%. The supplied voltage was kept at 10 kV and the tip-to-collector distance (TCD) was kept at 12 cm. The resulting nanofibers were dried at 80°C in vacuum condition for 24 h.

Measurement and Characterization

Viscosity and Conductivity of PVA/CS Blending Solution. Rotational viscometer (NDJ-1, China) was used to test the viscosity of PVA/CS solution. The conductivity of PVA/CS solution was measured by electric conductivity meter (LDD-801, China).

Morphology and Structure. The morphologies of samples were examined on a field scanning electron microscopy (SEM) (Jeol JSM-6700F, Japan) by applying an accelerating voltage of 20 kV on specimen sputter-coated with gold. The fiber diameter was measured by software from SEM micrograph. The diameters datum of electrospun fibers were an average of 50 data randomly taken from different spots of fibers.

Fourier transform-infrared spectroscopy (FT-IR) study was completed with a Nicolet 6700 spectrometer (Thermo, USA), using KBr pellets. X-ray photoelectron spectroscopy (XPS) analysis was performed by Mg Kα radiation with an ESCALAB 250 (Thermo-VG Scientific, USA) X-ray photoelectron spectrometer. X-ray diffraction (XRD) analysis was performed on a D/MAX2500V diffractometer (Rigaku, Japan) using Cu Kα radiation ($\lambda = 0.15418$ nm) to determine the crystal phase of the obtained samples.

Thermal Stability. TGA 209 thermogravimetric analyzer (Netzsch, Germany) was used to measure the weight loss of the samples within a certain temperature range. The samples were heated up to 800°C at a constant heating rate of 10°C/min under nitrogen flow at rate of 50 mL/min.

UV-Vis Analysis. UV-Vis spectrophotometer (Cary 5000, Varian) was used to measure the absorption spectrum of samples in the wavelength range from 200 to 2000 nm.

***In Vitro* Degradation.** The *in vitro* degradations of nanofibrous membranes were carried out in phosphate buffered saline (PBS, pH 7.4) at 37°C. The square-shaped specimens (10 mm × 10 mm) were immersed in test tubes containing 10 mL PBS and incubated in a water bath. At predetermined intervals, each sample was rinsed with distilled water to remove the residual PBS, and then dried in a vacuum oven maintained at 80°C to constant weight. The weight loss was calculated according to the following equation:

$$\text{Weight loss } (\%) = \frac{m_0 - m_t}{m_0} \times 100\% \quad (1)$$

where m_t is the weight of specimen at predetermined time and m_0 is the initial weight of specimen.

Assay of Antibacterial Activity in Liquid Culture. The assay of antibacterial activity of the medicated membranes against *S. aureus* was performed in liquid culture. In order to obtain the calibration curve, the concentration of the rejuvenated *S. aureus* suspension was set as 1.0. The absorbance for each sample (Relative concentrations of *S. aureus* at 0.1, 0.2, 0.3, and 0.4) was measured at 600 nm by the ultraviolet spectrophotometer (UV-754PC, China). On the basis of experimental data, a linear regression equation from calibration curve was determined as follows:

$$Y = 2.4956X + 0.0384 (R^2 = 0.998) \quad (2)$$

where the X is relative concentration of *S. aureus*, and Y is absorbance.

The medicated membranes with a weight of 20 mg (±0.2 mg) were sterilized by ultraviolet light for 30 min, and then those membranes were added into liquid culture medium containing 1 mL rejuvenated bacterial suspension and 9 mL KMB broth, respectively. After incubated on a shaker platform (100 rpm, 37°C) for 24 h, the absorbance of the medium was measured by an ultraviolet spectrophotometer at 600 nm and the relative concentration of *S. aureus* was calculated based on eq. (2).

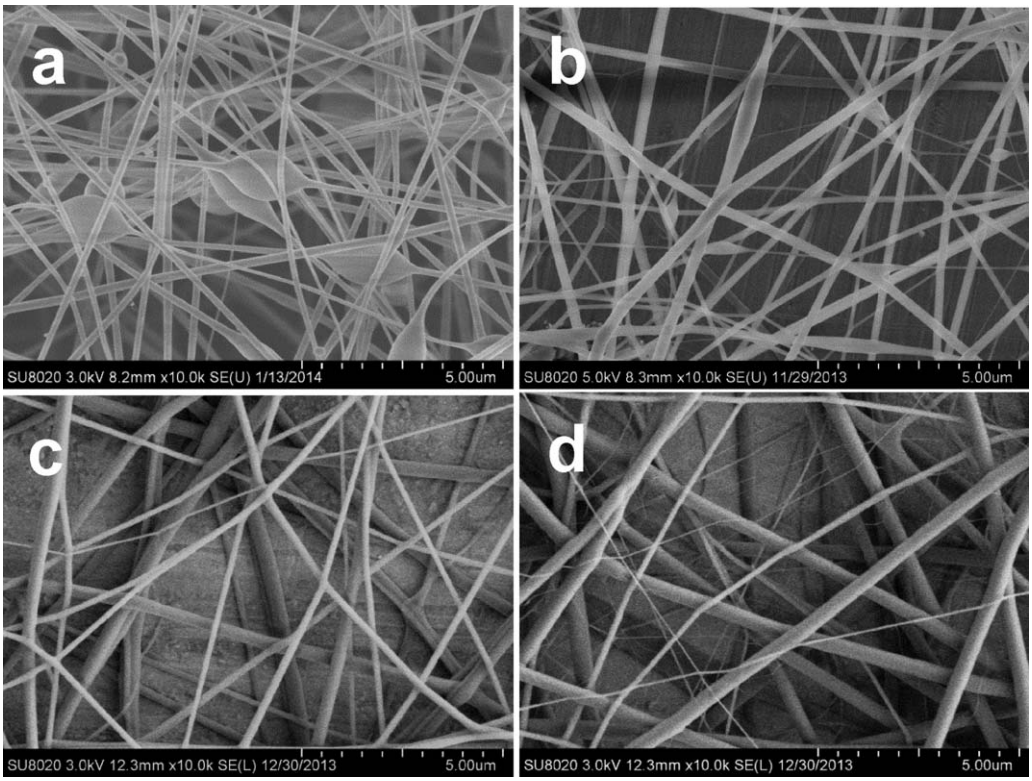

Figure 1. SEM photographs of PVA/CS nanofibers with the weight ratios of PVA/CS at (a) 1 : 1, (b) 2 : 1, (c) 3 : 1 and (d) 4 : 1.

Release Behavior. The release amount of Tet was performed in PBS (pH 7.4, 37°C). The absorbance at 360 nm for each solution was measured by an ultraviolet spectrophotometer (PBS solution as reference). On the basis of experimental data, the linear regression equation from the calibration curve was determined as follows.

$$Y = 0.4183X + 0.01927 \quad (R^2 = 0.9900) \tag{3}$$

where X is Tet concentration (mg/mL) and Y is absorbance.

The release behavior of medicated nanofibers was studied in PBS (pH 7.4, 37°C). 20 mg (± 0.2 mg) samples were immersed into test tubes containing 10 mL PBS, and then the test tubes were shaken on a shaker platform (100 rpm, 37°C). At designated time intervals, 5 mL supernatant was withdrawn from the release medium and 5 mL fresh PBS buffer solution was added into. The absorbance was measured using an ultraviolet spectrophotometer at 360 nm and the cumulative release percentage of Tet at various times was determined based on eq. (3).

The accumulative percentage of Tet release was calculated and plotted versus time using the following equation:

$$\text{Accumulative release}(\%) = \frac{W_{dr}(t)}{W_d} \times 100\% \tag{4}$$

where $W_{dr}(t)$ is the released Nisin at time t and W_d is the total entrapped Tet.

Statistical Analysis

Each experiment was repeated three times. Statistical analysis was performed using the unpaired Student's t-test, and the results were expressed as the means ± standard deviation (SD). A value of $p < 0.05$ was considered to be statistically significant.

RESULTS AND DISCUSSION

Viscosity, Conductivity, and Fiber Formability of PVA/CS Blend Solution

Appropriate PVA/CS ratio is very important to fabricate drug carrier PVA/CS/ZrO_2 hybrid nanofibers, herein, the viscosity, conductivity, and fiber formability of PVA/CS blend solution as a function of PVA/CS weight ratio was explored. As is well known, CS is a cationic polysaccharide with amino groups at the C2 position that are ionizable under acidic or neutral pH conditions. Therefore, the morphology and diameter of nanofibers would be seriously influenced by the weight ratio of PVA/CS. The SEM images of PVA/CS nanofibers at different weight ratios were shown in Figure 1. Figure 1 shows the average diameter of PVA/CS nanofibers were about 185, 205, 240, and 305 nm, respectively. The fibers were interspersed with spindle-shaped beads when the weight ratio of PVA/CS was at 1 : 1 [Figure 1(a)], and the average diameter of PVA/CS nanofibers increased with the PVA/CS weight ratio increasing, meanwhile, the beads were disappearing gradually, and the fibers tended to be uniform and smooth. Notably, the fibers were presented uneven in size once more when the weight ratio PVA/CS reached 4 : 1 [Figure 1(d)]. With an aim at further investigating these behaviors, the viscosity, and conductivity as a function of the weight ratio of PVA/CS solution were shown in Figure 2. As expected, the conductivity of PVA/CS solution declined from 1.69 to 1.04 mS·cm^{-1} as the weight ratio of PVA/CS increased

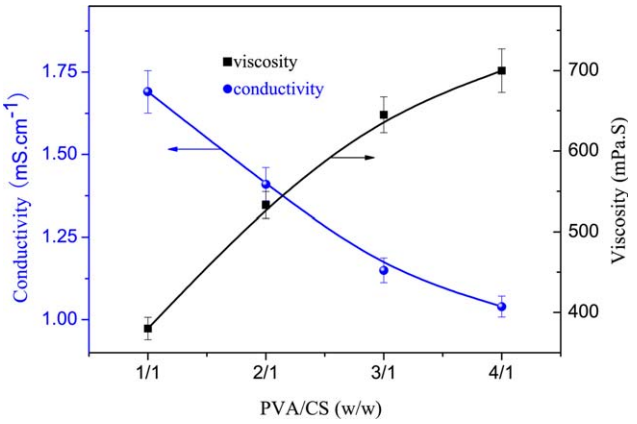

Figure 2. Conductivity and viscosity of PVA/CS blend solution. [Color figure can be viewed in the online issue, which is available at wileyonlinelibrary.com.]

from 1 : 1 to 4 : 1 because CS is anionic polyelectrolyte. As the charges carried by the jet increased, higher elongation forces were imposed to the jet under the electrical field. Because the overall tension in the fibers were dependent on the self-repulsion of the excess charges on the jet, as the charge density decreased, the diameter of the final fibers became wider.[5,29] As the weight ratio of PVA/CS was below 1 : 1, the repulsive force between ionic groups within the polymer backbone would inhibit the formation of continuous fiber during electrospinning, then electrospun fibers were uneven and interspersed with spindle-shape beads [Figure 1(a)].[30,31] The viscosity of PVA/CS solution was another important factor affecting the electrospinning process. As the weight ratio of PVA/CS changed gradually from 1 : 1 to 4 : 1, the viscosity of the solution was increased from 227 to 650 mPa·s. Within a certain degree, the improving of solution viscosity was conducive to produce smooth uniform nanofibers.[32] Nevertheless, as the weight ratio of PVA/CS beyond 4 : 1, the higher viscosity of solution resulted in the formation of uneven fibers because of the inability to maintain the flow of the solution at the tip of the needle. Therefore, the representative weight ratio of PVA/CS at 3 : 1 was chosen to prepare PVA-CS/ZrO_2 hybrid nanofibers.

Morphologies of Nanofibers

SEM photographs of PVA/CS/ZrO_2 hybrid nanofibers at different ZrO_2 contents are presented in Figure 3. PVA/CS nanofibers showed an average diameter of about 240 nm [Figure 3(a)], while these were 220 and 205 nm for PVA/CS/ZrO_2 hybrid nanofibers with ZrO_2 content at 20 and 40 wt %, respectively [Figure 3(b, c)]. It was illustrated that the average diameter of PVA/CS/ZrO_2 hybrid nanofibers decreased with the content of ZrO_2 increasing, because the viscosity of electrospun solution decreased with the addition of ZrO_2 sol owning to the lower viscosity of ZrO_2 sol. Although hydrogen bonds were formed among PVA, CS, and ZrO_2 units with the addition of ZrO_2 sol, this effect to increase the viscosity of solution could be ignored comparing with the decrease in viscosity causing by the addition of ZrO_2 sol. As ZrO_2 content reached 60 wt %, the fibers were interspersed with spindle-shape beads [Figure 3(d)] because of the lower viscosity.

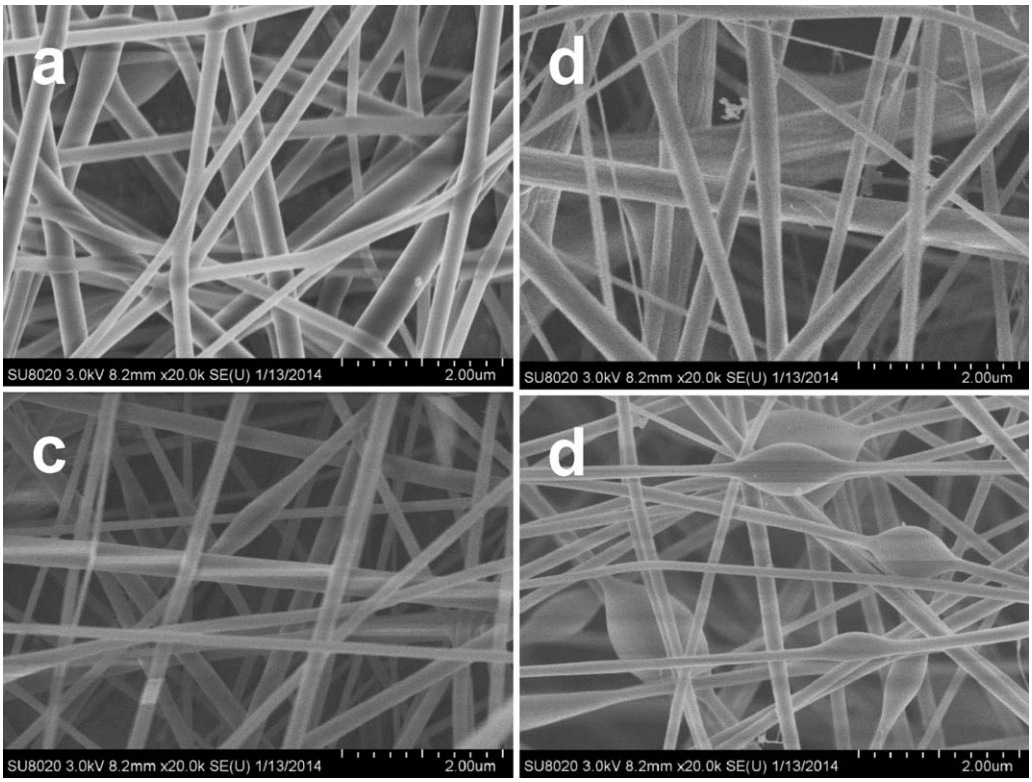

Figure 3. SEM photographs of PVA/CS/ZrO_2 hybrid nanofibers with ZrO_2 content at (a) 0, (b) 20, (c) 40 and (d) 60 wt %.

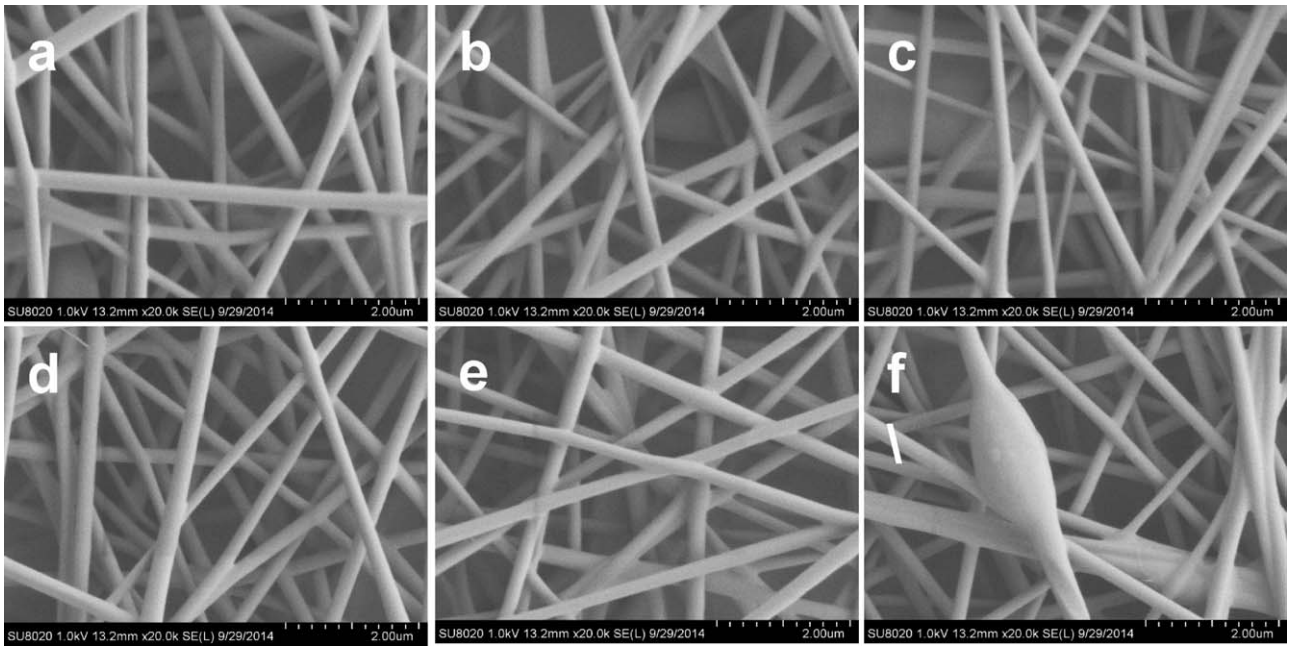

Figure 4. SEM photographs of Tet-PVA/CS/ZrO_2 hybrid nanofibers with Tet content at (a) 0, (b) 2, (c) 4, (d) 6, (e) 8, and (f) 10 wt %.

SEM photographs of Tet-PVA/CS/ZrO_2 nanofibers are presented in Figure 4. It could be clearly seen that no Tet particles were found on the surface of nanofibers, revealing that Tet has been dispersed evenly in nanofibrous matrix. Moreover, the Tet loading had no obvious effect on the morphology and size of the medicated nanofibers at Tet content below 8 wt % [Figure 4(a–e)]. Meanwhile, the nanofibers were interspersed with spindle-shaped beads when Tet content increased to 10 wt % [Figure 4(f)], owing to the poor compatibility of Tet with the carrier matrix.

Structure, Thermostability, UV Absorptivity, and Degradation of Drug Carrier

FT-IR Analysis. In order to investigate the interactions among PVA, CS, and ZrO_2 units, FTIR spectra measurements were taken (Figure 5). In the FTIR spectrum of PVA [Figure 5(a)], a characteristic peak of —OH stretching vibration was presented at 3378 cm^{-1}, and the —OH bending vibration was at 1432 cm^{-1}. The absorption peaks at 2937 and 1090 cm^{-1} were associated with C—H and C—O stretching vibrations, respectively, and 849 cm^{-1} was because of the C—C absorption peak. In the spectrum of CS [Figure 5(b)], the characteristic peaks for CS are present at 1655 (amide I, C=O stretching), 1597 (amide II, $—NH_2$, bending), and 1385 cm^{-1}($—CH_2$, bending).[33] A strong and broad band characteristic peak at 3450 cm^{-1} was associated with the stretching vibration for O—H, the extension vibration of N—H, and intermolecular hydrogen bonds of polysaccharide moieties. The bands at 902, 1025, 1081 cm^{-1} (C—O stretching), and 1156 cm^{-1} (asymmetric stretching of C—O—C bridge, glycosidic linkage) were because of its saccharide structure.[34,35] The band at 2875 cm^{-1} was associated with the bending vibration of —CH in $—CH_3$ from $—NHCOCH_3$. Furthermore, the band at 622 cm^{-1} was the crystallization peak.[36,37] As shown in Figure 5(c), a strong characteristic absorption band at 3416 cm^{-1} is assigned to the stretching vibration of —OH groups structured on ZrO_2, and an absorption band at 654 cm^{-1} is attributed to stretching vibration of Zr—O—Zr. In the spectra of PVA/CS/ZrO_2 nanofibers [Figure 5(d)], the characteristic absorption peak at 654 cm^{-1} of Zr—O—Zr was strengthened slightly, and the stretching vibration of —OH shifted from 3378 [Figure 5(a)], 3450 [Figure 5(b)], and 3416 cm^{-1} [Figure 5(c)] to low wavenumber at 3326 cm^{-1}, indicating that hydrogen bonds have formed among PVA, CS, and ZrO_2 units and active –OH groups structured on

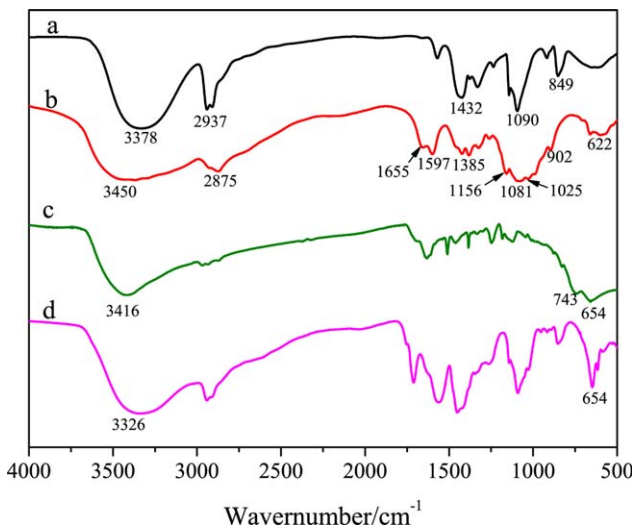

Figure 5. FT-IR spectra of (a) PVA nanofibers, (b) CS powders, (c) ZrO_2 nanofibers and (d) PVA/CS/ZrO_2 hybrid nanofibers (ZrO_2 40 wt %). [Color figure can be viewed in the online issue, which is available at wileyonlinelibrary.com.]

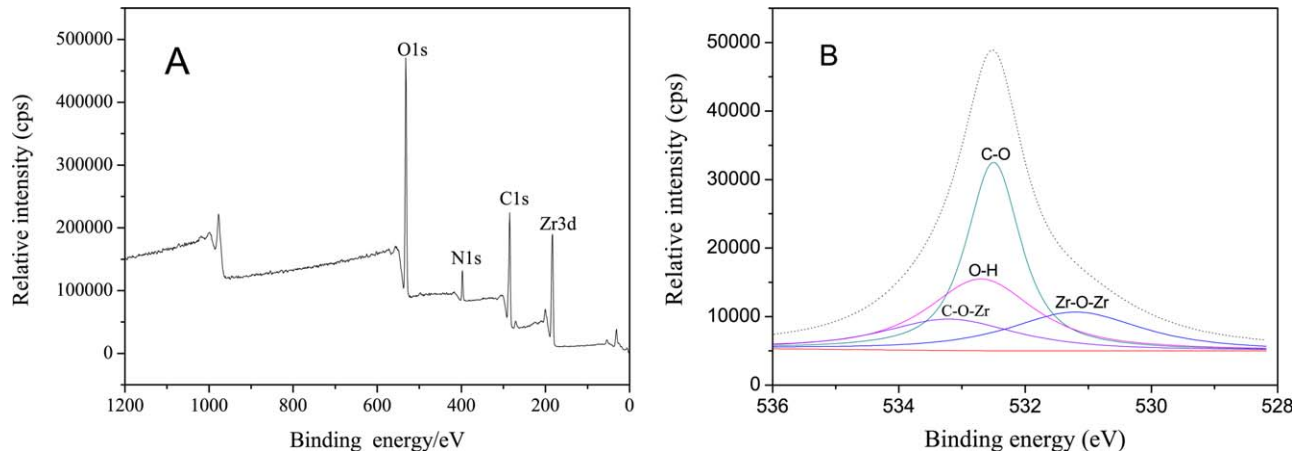

Figure 6. (**A**) XPS spectrum of PVA/CS/ZrO_2 hybrid nanofibers; (**B**) curve-fitted XPS C1s spectrum of the PVA/CS/ZrO_2 hybrid nanofibers (ZrO_2 40 wt %). [Color figure can be viewed in the online issue, which is available at wileyonlinelibrary.com.]

ZrO_2 units could react with PVA or CS molecular to form Zr—O—C bonds.

XPS Analysis. For further investigating composition and structure, the PVA/CS/ZrO_2 hybrid nanofibers with ZrO_2 content at 40 wt % was determined by XPS spectrum and the XPS full-scan spectra of the nanofibers are illustrated in Figure 6(A). As shown, peaks of C1s, O1s, N1s, and Zr3d were around 284.78, 532.39, 398.97, and 185.69 eV, respectively, indicating the existence of C, O, N, and Zr elements in the hybrid nanofibers. As shown in Figure 6(B), four peaks at about 531.2, 532.5, 532.7, and 533.2eV were assigned to Zr—O—Zr, C—O, O—H, and C—O—Zr when the peak O1s was fitted, revealing the formation of hybrid networks in PVA/CS/ZrO_2 polymeric matrix.

XRD Analysis. Figure 7 shows the XRD spectra of PVA nanofibers, CS powders, PVA/CS nanofibers, ZrO_2 nanofibers, and PVA/CS/ZrO_2 hybrid nanofibers, respectively. As shown, the PVA had two typical diffraction peaks appear at $2\theta = 11.4°$ and 19.4° because of the orthorhombic structure of PVA. The diffraction of CS powders showed a broad weak diffraction peak at $2\theta = 10.3°$ and a strong diffraction peak at $2\theta = 19.8°$. The diffraction of ZrO_2 nanofibers showed a peak at $2\theta = 4.6°$ and a broad peak at $2\theta = 26.5°$. As known, each component would have its own crystal regions in the nanofibers and the corresponding XRD spectra would be shown as simple superposition patterns of PVA and CS with the same ratio just like mechanical blend if there were no or weak interaction between them.[5] It could be seen clearly from the diffraction of PVA/CS nanofibers that the diffraction peak of PVA at $2\theta = 11.4°$ disappeared, moreover, the peak at $2\theta = 19.4°$ shifted to 20.3° and weakened, indicating that the presence of CS destroyed the crystal structure of PVA partially and formed strong hydrogen bond interactions between PVA and CS molecular chains in the composite polymeric matrix. In addition, the diffraction of PVA/CS/ZrO_2 hybrid nanofibers showed that the diffraction peaks of PVA and CS, as well as that of ZrO_2 nanofibers at $2\theta = 26.5°$ disappeared, implying that the incorporation of ZrO_2 units has destroyed further the crystal structure of PVA and CS, and formed hybrid networks in PVA/CS/ZrO_2 polymeric matrix.

Thermostability Analysis. PVA/CS nanofibers show four distinguishing stages in TG curve [Figure 8(A)]. Weight loss 10.8% between 20°C and 112.7°C was associated with the evaporation of free water and acetic acid, weight loss 8.7% between 112.7°C and 196.4°C was because of coordinated water and the chemical dehydration of hydroxyl condensation, weight loss 61.6% between 191.6°C and 348.2°C was mainly attributed to the chemical dehydration of the inner molecules and cleavage of C—O and C—C linkages, weight loss 17.7% between 348.2°C and 515.6°C was probably corresponding to the cleavages of C—N linkages, and beyond 515.6°C only the char residue remained. In sharp contrast to PVA/CS nanofibers, the PVA/CS/ZrO_2 hybrid nanofibers (ZrO_2 20 wt %) exhibited significant thermostability. As shown in Figure 8(B), it showed weight loss 10.9% at 20–135.1°C, 8.6% at 135.1–216.4°C, 55.2% at 216.4–403.6°C, 7.0% at 403.6–550.9°C and beyond 550.9°C, more

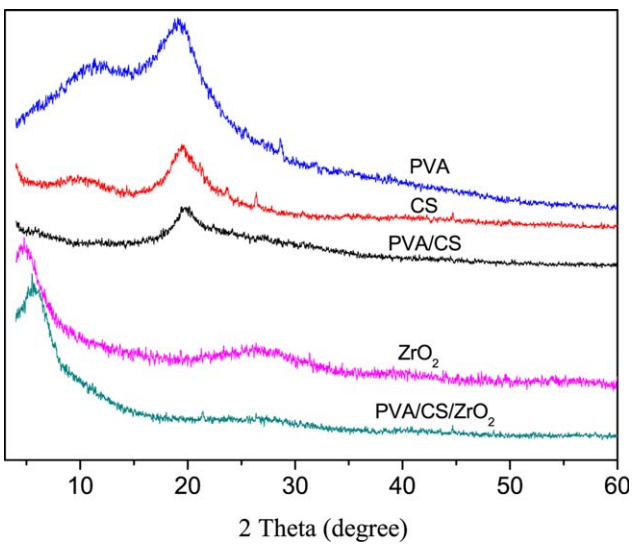

Figure 7. XRD spectra of PVA nanofibers, CS powders, PVA/CS nanofibers (PVA/CS=3 : 1), ZrO_2 nanofibers, and PVA/CS/ZrO_2 hybrid nanofibers (ZrO_2 40 wt %). [Color figure can be viewed in the online issue, which is available at wileyonlinelibrary.com.]

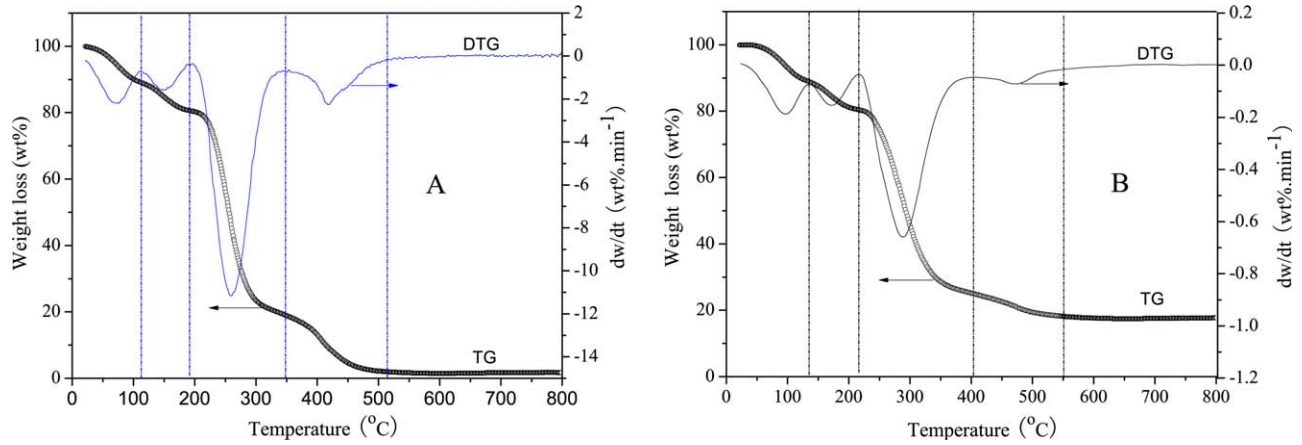

Figure 8. TGA curves of (**A**) PVA/CS nanofibers and (**B**) PVA/CS/ZrO_2 hybrid nanofibers (ZrO_2 20 wt %). [Color figure can be viewed in the online issue, which is available at wileyonlinelibrary.com.]

residues remains because of the addition of ZrO_2. It could be concluded from the data that the initial decomposition temperature of PVA/CS/ZrO_2 hybrid nanofibers was higher than that of PVA/CS nanofibers by 24.8°C in degree, indicating that the thermostability PVA/SPI nanofibers prominent increased with the addition of ZrO_2. The reason is that the hybrid networks in the polymeric matrix by the interactions of hydrogen or Zr—O—C bonds delay the decomposition process and increase the energy required to break the structure.

UV-Vis Spectra Analysis. UV-Vis spectra of PVA/CS/ZrO_2 nanofibrous membranes at different ZrO_2 contents are presented in Figure 9. The spectrum of PVA/CS shows no absorption in ultraviolet and near-infrared [Figure 9(a)], indicating that the ultraviolet light can transmit the PVA/CS nanofibrous membranes completely. In sharp contrast to PVA/CS, the spectrum of PVA/CS/ZrO_2 nanofibrous membranes shows an obvious absorption in ultraviolet region range 200–400 nm. In addition, the absorption in ultraviolet region increased with the increase of ZrO_2 content and the maximum absorption reached 7.89% with ZrO_2 content at 60 wt % [Figure 9(d)]. Meanwhile, the absorption of PVA/CS/ZrO_2 nanofibrous membranes increased in the near-infrared region range 400–2000 nm. As known, sunlight wavelength ranged from 200 to 400 nm was invisible ultraviolet light, which could cause photochemical reactions, creating radicals, and bond breakage resulting in polymeric matrix aging. While the ultraviolet shielding effect of ZrO_2 could effectively slow down the aging of polymeric matrix and prolong service life, as well as reduce the covered body harm from ultraviolet irradiation.

***In Vitro* Degradation.** As it is known, the degradation of drug carrier plays an important role in controlled drug release delivery system. Figure 10(A) illustrates the weight loss of PVA and PVA/CS/ZrO_2 membranes in PBS (37°C) and the corresponding change in pH value of PBS for PVA/CS/ZrO_2 membranes is depicted in Figure 10(B) (It is difficult to measure the weight of membranes when they have degraded into small fragments and dispersed in PBS, therefore, the degradation experimental time is set at 13 days. On the other hand, no change in pH value of PBS is observed for PVA membranes during degradation period).

As shown in Figure 10(A), both curves show no obvious weight loss in the first 5 days, and then increased seriously. Moreover, the weight loss of PVA/CS/ZrO_2 membranes was more than that of PVA at each designated time intervals. Within the first 5 days, water molecules were absorbed on the surface and diffused into the matrix of nanofibers. Correspondingly, the nanofibers were swollen and no obvious weight was observed. At this period, no change in pH value of PBS presented for PVA/CS/ZrO_2 membranes [Figure 10(B)]. Subsequently, the linkages of the matrix were weakened and the molecular chains of PVA or CS began to cleave resulting in a significant increase in weight loss. Furthermore, owing to the degradation of CS, pH value of PBS increased slightly for PVA/CS/ZrO_2 membranes. In general, semicrystalline polymers are composed of crystalline regions and amorphous regions. The degradation of semicrystalline polymers begins mostly from the amorphous regions, where the segments of the macromolecules pack more loosely and can be

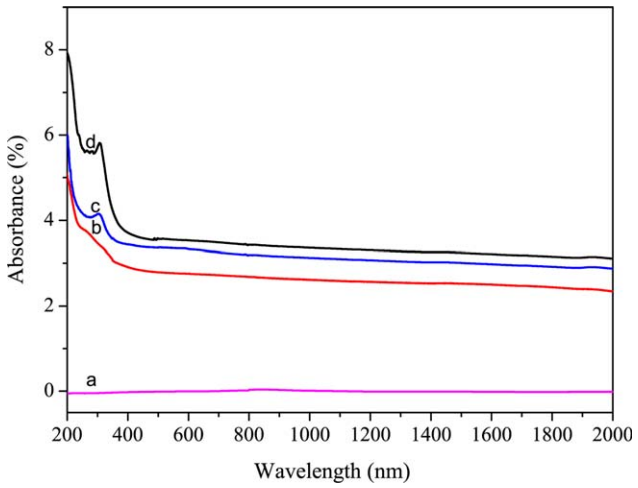

Figure 9. UV-Vis spectra of PVA/CS/ZrO_2 nanofibrous membranes with ZrO_2 contents at (a) 0, (b) 20, (c) 40, and (d) 60 wt %. [Color figure can be viewed in the online issue, which is available at wileyonlinelibrary.com.]

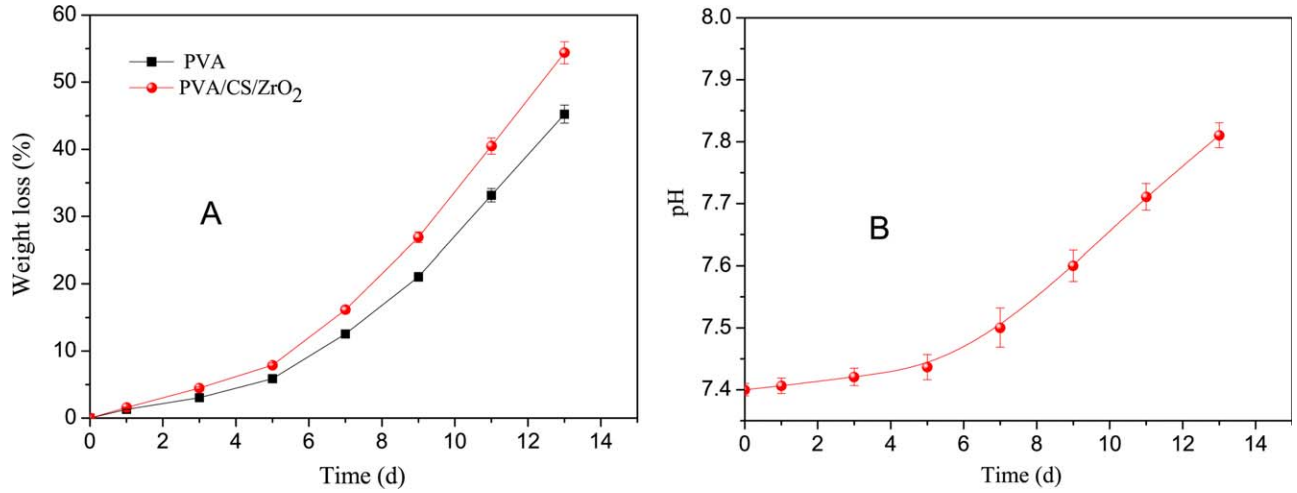

Figure 10. (**A**) Weight loss of nanofibers (in PBS at 37°C) and (**B**) pH changes of PBS for PVA/CS/ZrO_2 nanofibers (37°C). [Color figure can be viewed in the online issue, which is available at wileyonlinelibrary.com.]

more easily attacked by water molecules. As mentioned in XRD analysis, the PVA crystal structures were destroyed by the incorporation of CS and ZrO_2 units and caused a decrease in crystalline. Hence, the addition of CS and ZrO_2 could promote the degradation process.

Assay of Antibacterial Ability and Release Behavior for Tet-PVA/CS/ZrO_2 Nanofibers

Figure 11 presents the relative concentrations of *S. aureus* for Tet-PVA/CS/ZrO_2 nanofibrous membranes with different Tet content in liquid culture after incubation for at 37°C for 24 h. It can be seen from Figure 11, the relative concentration of *S. aureus* decreased rapidly when Tet content increased from 0 to 8 wt %, and then decreased slightly. It is well known that the antimicrobial activity is inversely proportional to the relative concentration of *S. aureus*. The amount of Tet released into bacterial suspension increased in quantity with the increase of the Tet content, which could inhibit the growth of *S. aureus* effectively and caused a rapid decrease in the relative concentration of *S. aureus* at Tet content below 8 wt %. At Tet content above 8 wt %, the increase of antimicrobial activity against *S. aureus* was slightly.

Experiments for the drug release characteristics from medicated nanofibers were carried out in PBS (pH 7.4, 37°C) and the accumulative release percentage of Tet from Tet-PVA/CS/ZrO_2 nanofibers was depicted in Figure 12(A). It is indicated that the accumulative release percentage depends on the total Tet incorporated into the fibers, similar to previously reported fibers loaded with several drugs.[38,39] Specially, the higher the fibers content in Tet, the greater the accumulative release percentage. The sample with the lowest Tet content (2 wt %) released only 71.4% of its total Tet within 84 h, whereas the sample with the highest Tet content (10 wt %) released 86.5% of its entrapped Tet. The networks with strong interaction formed among PVA, CS, and ZrO_2 units may be partially destroyed by the incorporation of Tet, therefore, the increase of Tet content causes an increase in the release percentage of Tet.

Tet released from medicated fibers shows a slight initial burst in each cumulative release percentage curve within first 5 h, mainly because of the dissolution of Tet on or near the surface of nanofibers. Afterwards, a gradual increase in the accumulative release follows, because the entrapped Tet molecules would take longer time to be released from inner core of the fiber matrix. Similar release profiles for chloroamphenicol from fibers were reported in our previous research.[27]

The mechanism governing drug release kinetics from degradable matrices is complex owing to alterations in polymer phase properties during degradation, causing changes in drug diffusivity and permeability with time.[40] Two representative mechanisms were reported on the release characteristics from nanofibers: one is desorption limited release,[41–43] the other is Fickian diffusion ($M_t/M_\infty < 0.6$).[38,44,45] In the present work, Fickian diffusion model for $M_t/M_\infty < 0.6$ was adopted as follows:

$$\frac{M_t}{M_\infty} = kt^n \tag{5}$$

where M_t is the accumulated amount of drugs released at an arbitrary time t, M_∞ is the accumulation amount of drugs

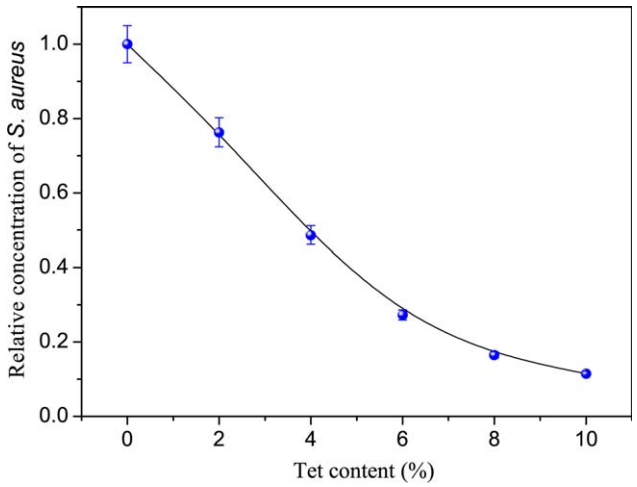

Figure 11. Relative concentrations of *S. aureus* in the samples propagated at 37°C for 24 h. [Color figure can be viewed in the online issue, which is available at wileyonlinelibrary.com.]

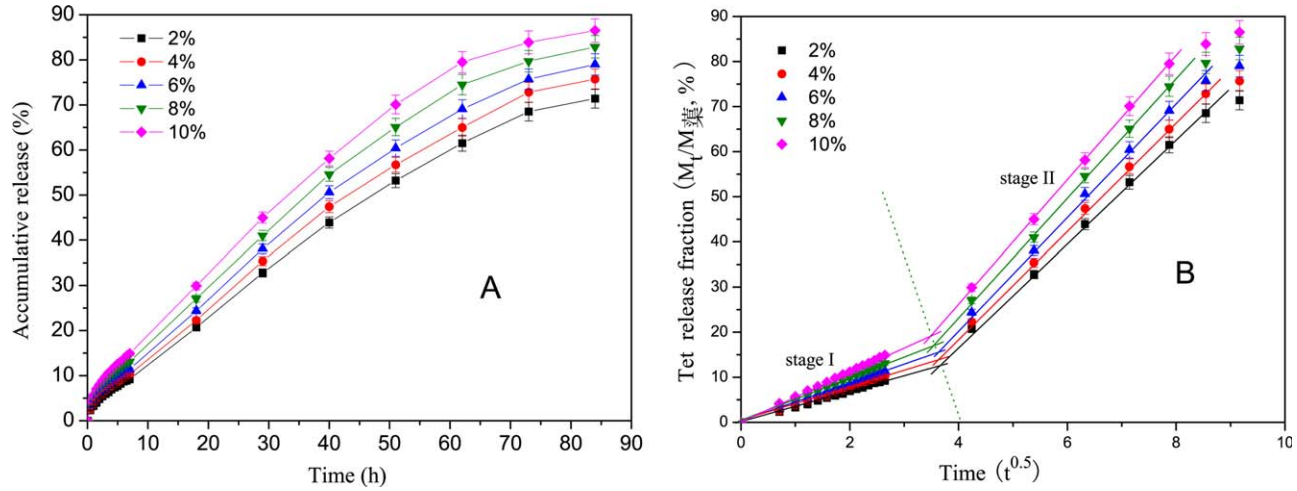

Figure 12. (**A**) Accumulative amount of Tet released from medicated nanofibers (pH 7.4, 37°C) and (**B**) Tet release curves of medicated nanofibers, re-plotted versus t^{5} for kinetic studies. [Color figure can be viewed in the online issue, which is available at wileyonlinelibrary.com.]

released at an infinite time (or the total amount of drug entrapped), n is diffusion index indicating the nature of release mechanism, and k is the constant characteristic of the drug/carrier system. A value of $n = 0.5$ shows the Fickian diffusion is observed and the fractional accumulative amount of release drug depends on $t^{0.5}$.

The released fraction of Tet a function of t^{5} from medicated fibers is illustrated in Figure 12(B). Each Tet release profiles consisted of two sequential stages. Furthermore, linear relationships ($R^2 > 0.995$) between M_t/M_{∞} and t^{5} were obtained for both stages, and the slope of the linear line for stage I was steeper than that of stage II. For the stage I, Tet molecules dispersed on surface of medicated nanofibers and absorbed or loosely bind near the surface of the nanofibers would diffuse quickly at initial release time. The slower release rate for stage II might be because of the Tet molecules entrapped into the inner core of the fiber matrix, which would take more time to be released because of the internal structure of the fiber need some time to become loose and the longer distance for Tet to diffuse through. Notably, the intersection of the two linear lines for each Tet release profiles shifted slightly to lower t^{5} with the increase of Tet content owing to the easy release at higher Tet content.

CONCLUSIONS

In the present study, Tet-PVA/CS/ZrO_2 nanofibers were fabricated *via* electrospinning technique. The viscosity and conductivity of PVA/CS blend solution depended on the weight ratio of PVA/CS. The increase of PVA/CS ratio showed a disappearance of spindle-shape beads and an increase in average diameter of the PVA/CS nanofibers, and a ratio of PVA/CS at 3 : 1 was suitable to fabricate drug carrier PVA/CS/ZrO_2 hybrid nanofibers. The fibers showed a decrease in average diameter with the increase of ZrO_2 content, and the nanofibers were uneven and interspersed with spindle-shape beads with ZrO_2 content at 60 wt % and above. The hybrid networks derived from PVA, CS, and ZrO_2 units in polymeric matrix were confirmed, and the incorporation ZrO_2 could improve the thermal stability of the hybrid fibers and endow them with an ultraviolet shielding effect ranged from 200 to 400 nm. The Tet loading dosage showed no obvious influence on the morphology and size of the medicated nanofibers at Tet content below 8 wt %, whereas the fibers were interspersed with spindle-shaped beads when Tet content increased to 10 wt %. The Tet-PVA/CS/ZrO_2 nanofibers exhibited well controlled release and better antimicrobial activity against *S. aureus*, and the Tet release from the medicated nanofibers could be described by Fickian diffusion model for $M_t/M_{\infty} < 0.6$. The encouraging results show that the Tet-PVA/CS/ZrO_2 nanofibers have potential for a wide range of biomedical applications in drug delivery and wound dressing.

ACKNOWLEDGMENTS

Financial support from National Natural Science Foundation of China (31171788 and 31371859) is acknowledged.

REFERENCES

1. Bagherzadeh, R.; Latifi, M.; Najar, S. S.; Gorji, M.; Kong, L. *Text. Res. J.* **2012**, *82*, 70.
2. Bagherzadeh, R.; Latifi, M.; Najar, S. S.; Kong, L. *J. Biomed. Mater. Res. A* **2013**, *101*, 765.
3. Bagherzadeh, R.; Najar, S. S.; Latifi, M.; Kong, L. *J. Biomed. Mater. Res. A* **2013**, *101*, 2107.
4. Bagherzadeh, R.; Latifi, M.; Kong, L. *J. Biomed. Mater. Res. A* **2014**, *102*, 903.
5. Jia, Y.-T.; Gong, J.; Gu, X.-H.; Kim, H.-Y.; Dong, J.; Shen, X.-Y. *Carbohydr. Polym.* **2007**, *67*, 403 2007.
6. Bagherzadeh, R.; Latifi, M.; Najar, S. S.; Kong, L. *J. Ind. Text.* **2014**, *43*, 496.
7. Park, J.-H.; Ju, Y.-W.; Park, S.-H.; Jung, H.-R.; Yang, K.-S.; Lee, W.-J. *J. Appl. Electrochem.* **2009**, *39*, 1229.
8. Ren, G.; Cai, F.; Li, B.; Zheng, J.; Xu, C. *Macrom. Mater. Eng.* **2013**, *298*, 541.

9. Kakade, M. V.; Givens, S.; Gardner, K.; Lee, K. H.; Chase, D. B.; Rabolt, J. F. *J. Am. Chem. Soc.* **2007**, *129*, 2777.
10. Unnithan, A. R.; Barakat, N. A.; Tirupathi Pichiah, P.; Gnanasekaran, G.; Nirmala, R.; Cha, Y.-S.; Jung, C.-H.; El-Newehy, M.; Kim, H. Y. *Carbohydr. Polym.* **2012**, *90*, 1786.
11. Gu, S.-Y.; Zou, C.-Y.; Zhang, C.-Y.; Ren, J. *Polym. Mater. Sci. Eng.* **2008**, *11*, 048.
12. Kanawung, K.; Panitchanapan, K.; Puangmalee, S.-o.; Utok, W.; Kreua-Ongarjnukool, N.; Rangkupan, R.; Meechaisue, C.; Supaphol, P. *Polym. J.* **2007**, *39*, 369.
13. Hu, J.; Wei, J.; Liu, W.; Chen, Y. *Biomater. Sci. Polym. Ed.* **2013**, *24*, 972.
14. Naveen, N.; Kumar, R.; Balaji, S.; Uma, T.; Natrajan, T.; Sehgal, P. *Adv. Eng. Mater.* **2010**, *12*, B380.
15. Kim, M. S.; Park, S. J.; Gu, B. K.; Kim, C.-H. *J. Nanomater.* **2012**, *2012*, 10.
16. Zhang, R.; Xu, W.; Jiang, F. *Fiber. Polym.* **2012**, *13*, 571.
17. Krajewska, B. *Sep. Purif. Technol.* **2005**, *41*, 305.
18. Mi, F.-L.; Tan, Y.-C.; Liang, H.-F.; Sung, H.-W. *Biomaterials* **2002**, *23*, 181.
19. Mi, F.-L.; Shyu, S.-S.; Wu, Y.-B.; Lee, S.-T.; Shyong, J.-Y.; Huang, R.-N. *Biomaterials* **2001**, *22*, 165.
20. Butler, B.; Vergano, P.; Testin, R.; Bunn, J.; Wiles, J. *J. Food Sci.* **1996**, *61*, 953.
21. Singh, B.; Sharma, V. *Int. J. Pharm.* **2010**, *389*, 94.
22. Sung, J. H.; Hwang, M.-R.; Kim, J. O.; Lee, J. H.; Kim, Y. I.; Kim, J. H.; Chang, S. W.; Jin, S. G.; Kim, J.; Lyoo, W. S. *Int. J. Pharm.* **2010**, *392*, 232.
23. Zhou, Y.; Yang, D.; Chen, X.; Xu, Q.; Lu, F.; Nie, J. *Biomacromolecules* **2007**, *9*, 349.
24. Zhang, Y.; Huang, X.; Duan, B.; Wu, L.; Li, S.; Yuan, X. *Colloid Polym. Sci.* **2007**, *285*, 855.
25. Chrissafis, K.; Paraskevopoulos, K. M.; Papageorgiou, G. Z.; Bikiaris, D. N. *J. Appl. Polym. Sci.* **2008**, *110*, 1739.
26. Wu, S.; Li, F.; Wu, Y.; Xu, R.; Li, G. *Chem. Commun.* **2010**, *46*, 1694.
27. Wang, H.; Ma, X.; Li, Y.; Jiang, S.; Zhai, L.; Jiang, S.; Li, X. *Int. J. Biol. Macromol.* **2013**, *62*, 494.
28. Lin, C.-C.; Liu, X.-M.; Peyton, K.; Wang, H.; Yang, W.-C.; Lin, S.-J.; Durante, W. *Arterioscl. Throm. Vas.* **2008**, *28*, 739.
29. Zong, X.; Kim, K.; Fang, D.; Ran, S.; Hsiao, B. S.; Chu, B. *Polymer* **2002**, *43*, 4403.
30. Son, W. K.; Youk, J. H.; Lee, T. S.; Park, W. H. *Polymer* **2004**, *45*, 2959.
31. Wang, H.; Wang, W.; Jiang, S.; Jiang, S.; Zhai, L.; Jiang, Q. *Iran. Polym. J.* **2011**, *20*, 551.
32. Theron, S.; Zussman, E.; Yarin, A. *Polymer* **2004**, *45*, 2017.
33. Li, R.; Hu, P.; Ren, X.; Worley, S.; Huang, T. *Carbohydr. Polym.* **2013**, *92*, 534.
34. Ávila, A.; Bierbrauer, K.; Pucci, G.; López-González, M.; Strumia, M. *J. Food Eng.* **2012**, *109*, 752.
35. Sajomsang, W.; Ruktanonchai, U. R.; Gonil, P.; Warin, C. *Carbohydr. Polym.* **2010**, *82*, 1143.
36. Naveen Kumar, H.; Prabhakar, M.; Venkata Prasad, C.; Madhusudhan Rao, K.; Ashok Kumar Reddy, T.; Chowdoji Rao, K.; Subha, M. *Carbohydr. Polym.* **2010**, *82*, 251.
37. Wang, Q.; Du, Y. M.; Fan, L. H. *J. Appl. Polym. Sci.* **2005**, *96*, 808.
38. Kontogiannopoulos, K. N.; Assimopoulou, A. N.; Tsivintzelis, I.; Panayiotou, C.; Papageorgiou, V. P. *Int. J. Pharm.* **2011**, *409*, 216.
39. Wang, H. L.; Li, Y. N.; Jiang, S. W.; Zhang, P.; Min, S.; Jiang, S. T. *J. Appl. Polym. Sci.* **2014**, 131.
40. Puppi, D.; Piras, A. M.; Detta, N.; Dinucci, D.; Chiellini, F. *Acta Biomater.* **2010**, *6*, 1258.
41. Srikar, R.; Yarin, A. L.; Megaridis, C.; Bazilevsky, A.; Kelley, E. *Langmuir* **2008**, *24*, 965.
42. Khansari, S.; Duzyer, S.; Sinha-Ray, S.; Hockenberger, A.; Yarin, A.; Pourdeyhimi, B. *Mol. Pharmaceut.* **2013**, *10*, 4509.
43. Gandhi, M.; Srikar, R.; Yarin, A.; Megaridis, C.; Gemeinhart, R. *Mol. Pharmaceut.* **2009**, *6*, 641.
44. Taepaiboon, P.; Rungsardthong, U.; Supaphol, P. *Nanotechnology* **2006**, *17*, 2317.
45. Jannesari, M.; Varshosaz, J.; Morshed, M.; Zamani, M. *Int. J. Nanomed.* **2011**, *6*, 993.